Paleobiology, 47(4), 2021, pp. 666–679
DOI: 10.1017/pab.2021.13

PALEOBIOLOGY
A PUBLICATION OF THE Paleontological SOCIETY

Article

Did shell-crushing predators drive the evolution of ammonoid septal shape?

*Erynn H. Johnson**, *Briana M. DiMarco*, *David J. Peterman*, *Aja M. Carter*, *and Warren D. Allmon*

Abstract.—For centuries, paleontologists have sought functional explanations for the uniquely complex internal walls (septa) of ammonoids, extinct shelled cephalopods. Ammonoid septa developed increasingly complex fractal margins, unlike any modern shell morphologies, throughout more than 300 million years of evolution. Some have suggested these morphologies provided increased resistance to shell-crushing predators. We perform the first physical compression experiments on model ammonoid septa using controlled, theoretical morphologies generated by computer-aided design and 3D printing. These biomechanical experiments reveal that increasing complexity of septal margins does not increase compression resistance. Our results raise the question of whether the evolution of septal shape may be tied closely to the placement of the siphuncle foramen (anatomic septal hole). Our tests demonstrate weakness in the centers of uniformly thick septa, supporting work suggesting reinforcement by shell thickening at the center of septa. These experiments highlight the importance of 3D reconstruction using idealized theoretical morphologies that permit the testing of long-held hypotheses of functional evolutionary drivers by recreating extinct morphologies once rendered physically untestable by the fossil record.

Erynn H. Johnson[†] and Aja M. Carter[‡]. Department of Earth and Environmental Science, University of Pennsylvania, Philadelphia, Pennsylvania 19104, U.S.A. E-mail: erynnj@upenn.edu, caja@seas.upenn.edu. Present addresses: [†]Paleontological Research Institution, Ithaca, New York 14850, U.S.A. [‡]Electrical and Systems Engineering, University of Pennsylvania, Philadelphia, PA 19104, U.S.A.

Briana M. DiMarco. Department of Biology, Drexel University, Philadelphia, Pennsylvania 19104, U.S.A. E-mail: bmd78@drexel.edu

David J. Peterman[§]. Department of Earth and Environmental Sciences, Wright State University, Dayton, Ohio 45435, U.S.A. [§]Present address: Department of Geology and Geophysics, University of Utah, Salt Lake City, Utah 84112, U.S.A. E-mail: David.Peterman@utah.edu

Warren D. Allmon. Paleontological Research Institution, Ithaca, New York 14850, U.S.A.; and Department of Earth and Atmospheric Science, Cornell University, Ithaca, New York 14850, U.S.A. E-mail: wda1@cornell.edu

Accepted: 14 February 2021
*Corresponding author.

Introduction

Ammonoids, extinct, externally shelled (ectocochleate) cephalopods, have an extensive fossil record preserving their external coiled shells and complex interior shell walls (septa) (Daniel et al. 1997; Kerr and Kelley 2015; Lemanis et al. 2016a; Peterman and Barton 2019). These septa created gas-filled chambers within the shell that were used to regulate buoyancy. While their distant, modern relatives, the nautilids, have simple, sinuous septa that create similar chambers, ammonoids evolved intricately folded septa unlike any modern cephalopod morphologies (Fig. 1). Although cuttlefish have corrugated structures within their internalized shells, they represent highly modified, tiny pillars supporting parallel septa (Checa et al. 2015). Throughout their evolutionary history, ammonoids developed increasingly fractal complex septa (possessing scale-invariant geometry) before their extinction at the end of the Mesozoic (Boyajian and Lutz 1992; Landman et al. 2014, 2015; Tajika et al. 2018, 2020; Peterman and Barton 2019). Because these complex morphologies do not exist in modern mollusk shells, the mystery of why ammonoids invested the biological resources to generate fractal geometries has plagued paleontologists for centuries (Buckland 1836). Previous investigators have suggested

© The Author(s), 2021. Published by Cambridge University Press on behalf of The Paleontological Society. 0094-8373/21

https://doi.org/10.1017/pab.2021.13 Published online by Cambridge University Press

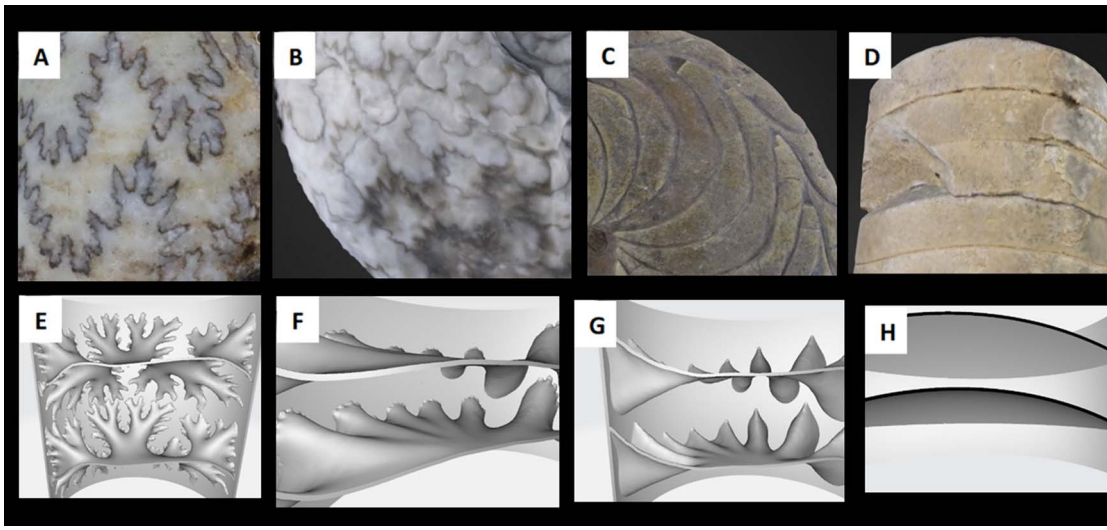


FIGURE 1. Fossil and model septa. Images showing cephalopod septa (inner chamber walls) and sutures (where septa meet the outer shell wall); complexity decreases from left to right. Top row: sutures visible on fossil cephalopods from the Paleontological Research Institution research collections: A, ammonite sutures on *Cadoceras sublaeve* (PRI 70580); B, ceratitic sutures on *Gymnotoceras beachi* (PRI 43629); C, goniatitic *Imitoceras rotatorium* (PRI 44566); D, nautiloid sutures on *Actinoceras beloitense* (PRI 70326). Bottom row: computer-generated models of cephalopod chambers, bisected to show cross section of septa. E, ammonitic septa of *Diplomoceras*; F, ceratitic septa of *Otoceras*; G, goniatitic septa of *Schistoceras*; H, nautiloid septa of *Eifeloceras*.

physiological relationships between septal complexity and respiration (Newell 1949), gas production (Pia 1923), liquid transport (Mutvei 1967), muscle attachment (Ebel 1992), soft body attachment (Lewy 2003), and rapid growth (Klug et al. 2008). Others have hypothesized mechanical relationships between septal complexity and buoyancy (Teichert 1967; Kulicki and Mutvei 1988; Saunders 1995; Daniel et al. 1997) or hydrostatic pressure (Buckland 1836; Hewitt and Westermann 1997; Hassan et al. 2002). More recently, Lemanis and colleagues (Lemanis et al. 2016b; Lemanis 2020) used finite element analysis to study the effect of increasing septal complexity on shell strength. These studies demonstrated that increasing complexity did not create increased resistance to hydrostatic pressure from surrounding water (Lemanis et al. 2016b; Lemanis 2020); however, it did increase resistance to point loads like those imparted by shell-crushing predators (Lemanis et al. 2016b; Lemanis 2020). Others (Daniel et al. 1997; Hassan et al. 2002) have made similar suggestions that increased septal complexity had a defensive purpose (e.g., increased chamber refilling), although this has yet to be demonstrated by investigators using evidence from the fossil record (Kerr and Kelley 2015). In contrast to functional interpretations of complex septa, some have postulated such shapes may have been generated by varying degrees of fabricational noise (for review, see Klug and Hoffmann 2015).

Both ammonoids and nautiloids are known to have fallen prey to shell-crushing predators including, fishes (hybodont sharks [Vullo 2011], ptychodontoid sharks [Romer 1966], Heterodontidae [sharks], Batoidea [rays] [Vermeij 1977], Pycnodontiformes, Semionotiformes, Macrosemiiformes, and Pholidophoriformes [Tintori 1998]), marine reptiles (placodonts [von Huene 1956], ichthyosaurs [Vermeij 1977], mosasaurs [Kauffman and Kesling 1960]), and even other cephalopods (Mapes and Chaffin 2003; Vullo 2011; Kerr and Kelley 2015; Takeda et al. 2016) (see also Richter 2009; Keupp 2012). To further test the hypothesis that predation pressures from shell-crushing predators drove the evolution of increasingly complex septa, we created novel physical models of various septal shapes to analyze their strengths in compression.

https://doi.org/10.1017/pab.2021.13 Published online by Cambridge University Press

The processes of fossilization often render morphologies physically untestable (e.g., trapping remains in rocks, changing their composition, loss of organic components, diagenesis), presenting a major challenge to understanding the form and function of extinct organisms. Paleontologists have engineered many creative means to handle this problem, including physical and virtual experimentation on real and model specimens (e.g., Schulp 2005; Crofts and Summers 2014; Kolmann et al. 2015; Lemanis and Zlotnikov 2018; Johnson and Carter 2019; Peterman and Barton 2019). In this study, we used computer-aided design to create 3D printable ammonoid models, each of which isolated a single chamber bound by two septal walls (Figs. 1, 2). Here, we present empirical data investigating relationships between septal complexity and shell strength to test whether increasingly complex septa provided increased resistance to compression by shell-crushing predators.

Materials and Methods

Experimental Design.—To understand the effects of increasing septal complexity on shell strength, we tested septa from four morphological groups. The first three septal types: ammonitic, ceratitic, and goniatitic, are septal shapes found in ammonoid fossils (Fig. 1A–C, E–G). Ammonitic septa are the most complex within the ammonoids (exhibiting fractal scaling), and goniatitic septa are the least complex (Arkell et al. 1957). The fourth septal morphology we tested represented nautiloid septa, which are simple and sinuous (these shapes are still seen in modern *Nautilus*) (Fig. 1D,H). We selected 12 genera representing these four septal types: *Diplomoceras*, *Baculites*, and *Douvilleiceras* (ammonitic); *Otoceras*, *Pearylandites*, and *Xenaspis* (ceratitic); *Schistoceras*, *Manticoceras*, and *Diaboloceras* (goniatitic); and *Eifeloceras*, *Endoceras*, and *Orthoceras* (nautiloid) (Table 1). We chose these genera due to their high disparity within each septal shape type. We quantified the complexity of these septa using the fractal box-counting method to generate scaling exponents (Peterman and Barton 2019; Table 1; see "Quantification of Sutural Complexity").

Additionally, we created a hypothetical control model with completely straight septa. For consistency, we created all models using a laterally compressed cylindrical shell with no whorl overlap or shell taper (Fig. 2) to prevent these factors from contributing to stress distribution. Previous authors believed that whorl overlap contributes to shell strength in buttressing against compression by a predator; thus, we decided to isolate the influence of septal shape only (Hewitt and Westermann 1997). We 3D printed our shells using brittle materials to maintain consistent material properties and normalize for size and shell thickness to control biological complications such as differences in microstructure and the thickness of ammonoid and nautiloid septa (Saunders 1995).

Model Creation.—Each of the 13 models consisted of a segment of a shell with a slightly laterally compressed whorl section (Fig. 2B). We constructed a single whorl section in the computer graphics software Blender 2.76 (Blender Online Community 2020) by creating a circle and scaling the transverse directions to yield a whorl height to whorl width ratio of 1.4. We extruded this whorl section in the longitudinal direction to create a thin mesh in 3D space. Next, we used the solidify modifier in Blender to extrude the model in the positive (outward) directions to define thickness. We held all thicknesses constant, because this property varies widely between different ectocochleates. We chose a thickness value of 1% whorl height based on baculitid septal measurements at 30 mm whorl height (Peterman et al. 2019).

We scanned suture patterns of each specimen from their original sources (Arkell et al. 1957; Jones 1963; Teichert 1967; Wright 1996; Peterman and Barton 2019). We mirrored complete hemisutures with their internal (dorsal) elements to create complete suture patterns. We then imported these sutures into Blender to reduce them to a 1D corrugated line within 3D space. We wrapped this object around the whorl section using the curve modifier in Blender and scaled in the longitudinal directions to prevent aberration from the original shape. We joined this suture pattern in 3D at the edges to create a ring, which we then extruded inward to a single point at the center of the septum. Afterward, we refined this crude

https://doi.org/10.1017/pab.2021.13 Published online by Cambridge University Press

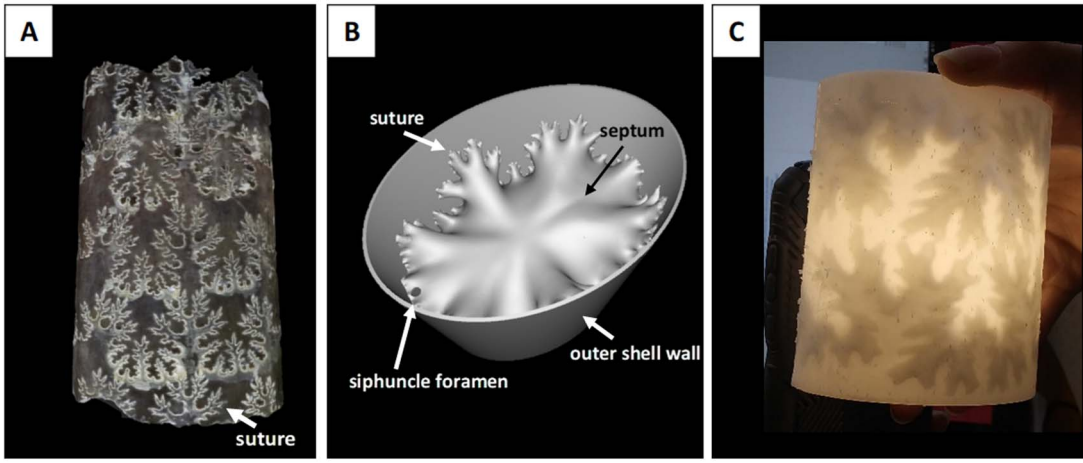


FIGURE 2. Fossil, computer-generated, and 3D-printed ammonoids. Comparison of fossil and model ammonoids. A, *Baculites* sp. (PRI 70605). Fossil is infilled such that suture lines remain visible. B, 3D *Baculites* model with slightly laterally compressed shell generated in Blender 2.76. C, 3D-printed *Diplomoceras* model created in Blender, printed on Formlabs Form 2.

septum to add additional vertices to the mesh. We selected the entire mesh (excluding the suture line) and then iteratively smoothed it to approximate a minimum curvature surface. We extruded this curved, 2D surface to 1% of whorl height to yield a single 3D mesh of each septum. We chose to maintain uniform thickness and to isolate the influence of septal shape on shell strength without introducing variations in strength owing to localized shell thickening. We duplicated 3D septa and transformed them to create the final models with two septa spaced according to their real-world counterparts. We could not hold septal spacing constant, because this would create unrealistic gaps or self-intersections due to the variability in longitudinal extent between different sutures. We scaled the external shell longitudinally to accommodate the septa for each species and then unified it with the Boolean modifier to produce a single manifold mesh suitable for 3D printing.

We created siphuncular foramina by subtracting a cylinder (representing the siphuncle) from the septal models with the Boolean modifier in Blender. We spaced all ventral siphuncles (present in almost all ammonoids) to 1% of whorl height from the venter (0.75 mm). We chose to maintain a constant position of the siphuncle foramina to maintain an experimental system in which we only tested the influence of septal shape on shell strength.

TABLE 1. Taxa used to make models. List of select septal types and representative genus and species whose sutures were used to create 3D models (Arkell et al. 1957; Jones 1963; Teichert et al. 1964; Wright 1996; Peterman and Barton 2019). Scaling exponents used to quantify complexity following Peterman and Barton (2019).

Suture type	Genus	Species	Scaling exponent	Standard error
Ammonitic	*Diplomoceras*	*notabile*	1.56	0.014
Ammonitic	*Baculites*	*compressus*	1.53	0.011
Ammonitic	*Douvilleiceras*	*monile*	1.44	0.007
Ceratitic	*Otoceras*	*woodwardi*	1.31	0.024
Ceratitic	*Pearylandites*	*troelseni*	1.27	0.015
Ceratitic	*Xenaspis*	*carbonarius*	1.24	0.018
Goniatitic	*Schistoceras*	*missouriense*	1.23	0.011
Goniatitic	*Manticoceras*	sp.	1.2	0.008
Goniatitic	*Diaboloceras*	*varicostatum*	1.19	0.004
Nautiloid	*Eifeloceras*	*kayseri*	1	0
Nautiloid	*Endoceras*	*abundum*	1	0
Nautiloid	*Orthoceras*	*regulare*	1	0

https://doi.org/10.1017/pab.2021.13 Published online by Cambridge University Press

Relocating the siphuncle foramen (a hole) would result in changing the position of a stress concentrator. Because siphuncle size varies widely within each of the examined taxa, we set the siphuncle size at a constant 2.5 mm (3.33% of whorl height, as measured from the baculitid specimen in Peterman et al. 2019).

3D Printing

We printed our models on a Formlabs Form 2 printer using Formlabs Rigid Resin at 50 µ resolution (Fig. 2C). We washed the models in a Form Wash with isopropanol for three successive intervals of 15 minutes each. In between washes, we drained excess isopropanol from the model chambers through the siphuncle foramen. Finally, we removed the models from the build platform using wire cutters and then cured them in Form Cure with UV light for 3 hours at 80°C.

Rigid resin does not behave in a brittle fashion if postprocessed following suggested Formlabs guidelines for curing. Therefore, we took extra steps to make sure our models had the appropriate material properties to model shell breakage accurately. We washed each model three times instead of once to ensure that as much excess resin was removed from the model's interior chambers as possible. Additionally, we tested several miniature models with the following curing times: 15 (Formlabs recommended), 30, 45, 60, 120, and 180 minutes. We found that the samples became brittle at 120 and 180 minutes of curing (see Supplementary Fig. S1). Thus, we used a 180 minute cure time in our final experiments to ensure brittle behavior.

Experiments.—We conducted compression experiments using an Instron Universal Testing Machine with a 2 kN load cell. We used two flat plates to mimic a vertebrate predator's theoretical flat crushing teeth (Fig. 3). This methodology is similar to that of Kolmann et al. (2015); those authors used curved aluminum plates to simulate the jaws of a durophagous predator. Using flat plates is the most general way to test prey strength in bulk compression without introducing numerous assumptions about the placement of point loads from specific predator dentitions. Shell strength varies based upon loading location (Johnson 2021). As the current literature lacks physical testing that isolates septal morphologies and relative strength, the goal of this study was to develop a first-order approximation for these relationships in bulk compression.

We lined the crushing plates with sandpaper to prevent the models from rolling and oriented the models so that both the shortest axis of the outer shell and the septa were perpendicular to the plates. This was a biologically realistic choice, because predators are generally most likely to crush prey over their smallest axis (Stein et al. 1984). We then surrounded the experimental setup with a protective shield and lowered the top plate at 3 mm per minute, creating a quasistatic loading regime. A computer continuously recorded the force of the model pushing back on the top plate. We confirmed brittle behavior in the load-displacement curves, because the shell models demonstrated largely linear elastic behavior with only small regions of plasticity during initial loading and immediately before reaching peak load. Upon reaching peak load, shells shattered and came out of contact with the top plate, causing a drastic drop in load read by the machine. For each genus, we conducted five trials (except in the cases of *Douvilleiceras*, *Otoceras*, *Diaboloceras*, and *Eifeloceras*, where we had six trials because an extra print was available for each). We conducted statistics for peak load comparisons, including the Shapiro-Wilks normality test, Kruskal Wallis test, and Dunn post hoc tests, in R (R Core Team 2020).

Quantification of Sutural Complexity.—We quantified the complexity of each suture pattern using the fractal box-counting method (see Peterman and Barton 2019; Supplementary Fig. S2). We used the software Benoit 1.3 to compute the scaling exponent of each hemisuture of the chosen specimens. This metric quantifies the degree to which a pattern fills space and scales as a function of size. Fractal box-counting involves superimposing a grid over a pattern and measuring the number of boxes occupied by that pattern at various scales (box sizes). As box size decreases, the number of occupied boxes increases. The rate at which these occupied boxes increase at smaller scales is equal to the scaling exponent (i.e., the slope

https://doi.org/10.1017/pab.2021.13 Published online by Cambridge University Press

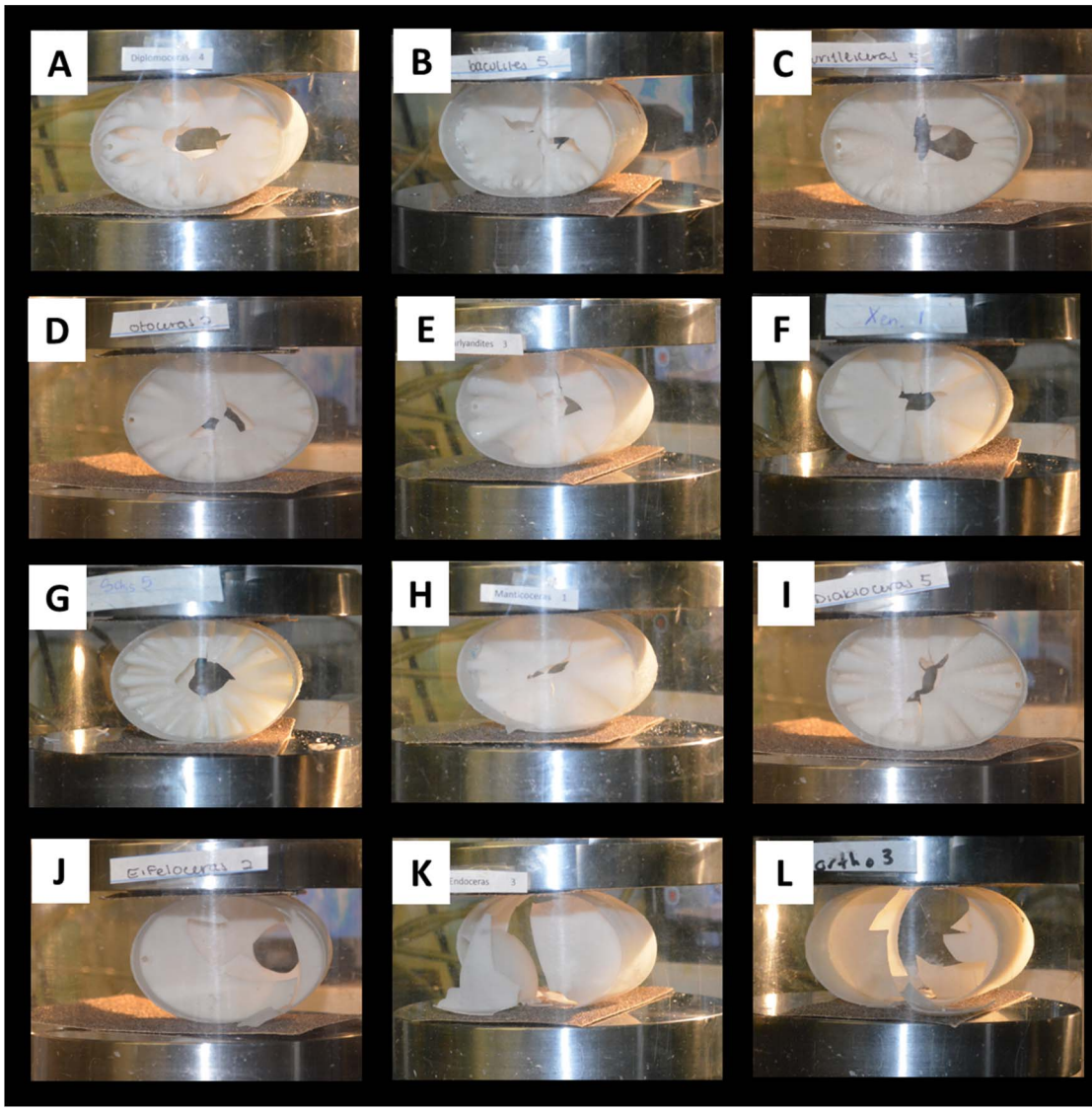


FIGURE 3. Models in compression. Sample images of models during compression tests in Instron Universal testing machine. Instron plates are lined with sandpaper. Top row: ammonitic models A, *Diplomoceras*; B, *Baculites*; C, *Douvilleiceras*. Second row: ceratitic models D, *Otoceras*; E, *Pearylandites*; F, *Xenaspis*. Third row: goniatitic models G, *Schistoceras*; H, *Manticoceras*; I, *Diaboloceras*. Bottom row: nautiloid models J, *Eifeloceras*; K, *Endoceras*; L, *Orthoceras*.

of a power function fit through the sampled data points). We remediated directional bias by rotating the grid every 5° and counting the minimum number of occupied boxes at each step size. We excluded data points below 10 pixels, the approximate width of each digital hemisuture, from each analysis.

It should be noted that the fractal box-counting method is most appropriate for fractal objects or those approximating fractal scaling and self-similarity. The ceratitic, goniatitic, and nautiloid sutures do not exhibit self-similarity and are not true fractals. Nonetheless, their data points are well fit by power functions with low standard errors (Table 1). While such patterns cannot be interpreted as fractals sensu stricto, scaling exponents adequately approximate their complexity in terms of the relative amount of space filled by each hemisuture.

https://doi.org/10.1017/pab.2021.13 Published online by Cambridge University Press

Statistical Analysis.—We conducted all statistical analyses in R (2020). We first used the Shapiro-Wilks test ($p < 0.05$) to determine if our data had a normal distribution. It did not; we, therefore, used a Kruskal-Wallis test ($p < 0.05$) and post hoc Dunn test ($p \leq 0.025$) in place of analysis of variance tests. We conducted five to six trials for each of the 13 model septal types.

Results

The 3D-printed models reflected an accurate first-order approximation for shell failure based upon their brittle behavior in compression, exhibiting dominantly linearly elastic behavior with only minor regions of plasticity upon initial loading and directly before failure (breakage) (Fig. 4B). This observation verified that the models' peak loads were appropriate proxies for the relative strengths of different shell morphologies (Johnson 2020, 2021). Additionally, we used the shapes of the load-displacement curves to assess any differences in the mechanical behavior of various septal shapes upon loading.

Peak Load.—Comparisons of ammonitic, ceratitic, goniatitic, nautiloid, and straight septa yielded only two significant pairwise differences (Kruskal-Wallis p-value = 0.04567). These comparisons showed that straight septa models (representing controls) were significantly stronger than ammonitic septa (Dunn test $p = 0.0019$) and goniatitic septa (Dunn test $p = 0.0070$) (Fig. 4). The peak loads of models representing different genera also demonstrated significant differences summarized in Table 2 (Kruskal-Wallis p-value = 2.195e-07, significant Dunn test pairwise comparisons $p \leq 0.025$) (Fig. 5A, Supplementary Fig. S3).

Loading Observations and Fracture Location.—During the experimental trials, we observed cracks in some models before complete failure after peak load was reached (e.g., *Diplomoceras*, *Douvilleiceras*, *Diaboloceras*, and *Manticoceras*). These cracks are visible as small dips on the load versus displacement curve (Fig. 5B–E). Ammonitic, ceratitic, and goniatitic models (ammonoid morphologies) consistently showed crack propagation from the top and bottom of the model where the plates were in contact toward the center of each septum (Fig. 3A–I). Upon failure, the center of one or both septa frequently shattered. In the case of nautiloid septa (nautiloid morphologies) and straight septa (control morphology), we saw cracks in differing positions on the septa, some through the center of a septum, others toward the margins of a septum near the outer shell, and some that caused septa to break almost entirely free from the outer whorl wall (Fig. 3J,K). In all cases, cracks propagated through septa before the outer shell (cylindrical tube) began to crack.

Discussion

Using brittle 3D-printed materials allows for the relative comparison of the strength provided by different septal shapes (3D-printed models should not be used to infer the absolute magnitude of shell strength in life). While computational modeling methods (e.g., finite element analysis) have also proven useful to test extinct morphologies, it becomes increasingly difficult to accurately model the fracture and failure of shapes as the extinct morphologies increase in complexity. Thus, digital models typically yield stress distributions rather than modeling failure itself (Lemanis et al. 2016b). By using physical models, we tested failure without these restrictions. These 3D-printed materials exhibit brittle behavior consistent with mechanical tests conducted on mollusk shells in previous studies (e.g., Kolmann et al. 2015). While this study represents an idealized experimental setting with theoretical predators and prey, the compression tests performed here provide the best first-order approximation of septal shape and shell strength relationships so far provided by empirical testing.

Peak Load.—Straight septa (representing controls) were stronger than ammonitic and goniatitic septa. However, there was no significant difference between models of real septal types (ammonitic, ceratitic, goniatitic, or nautiloid) (Fig. 4). In other words, ammonoid septa were not more resistant to crushing than nautiloid septa, and more complex ammonoid septa (those with higher scaling exponents) were not more resistant than less complex ammonoid septa (those with lower scaling

https://doi.org/10.1017/pab.2021.13 Published online by Cambridge University Press

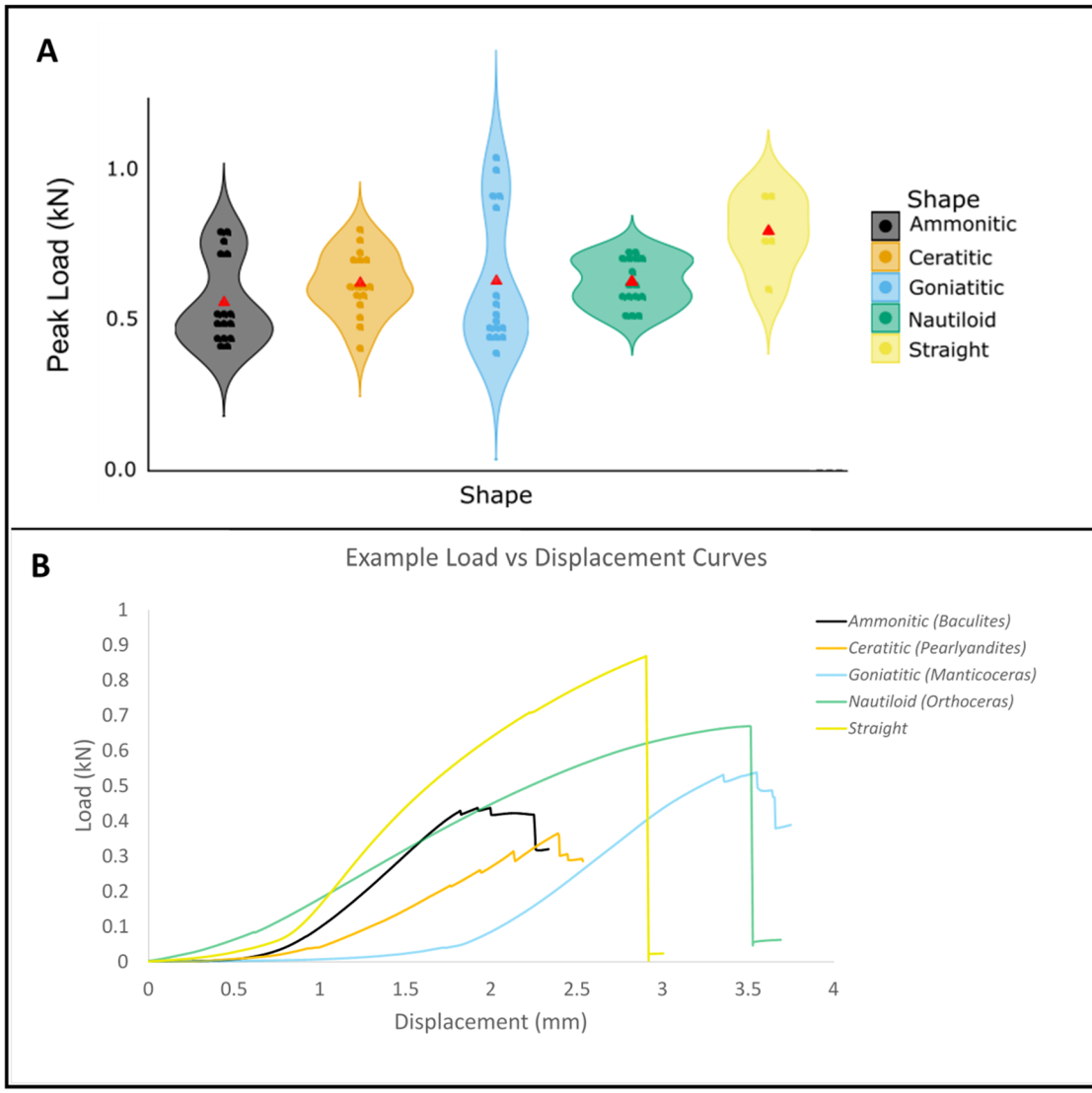


FIGURE 4. Septal shape and peak load sustained. A, Violin plot peak load (kN) sustained by models with different septal types decreasing in complexity from left to right: ammonitic, ceratitic, goniatitic, nautiloid, and straight (control). Width of spindles indicates distribution of data points. Means for each septal shape are represented by red triangles. Straight septa (representing controls) were stronger than ammonitic and goniatitic septa ($p \leq 0.025$). There was no significant difference between models of real septal types (ammonitic, ceratitic, goniatitic, or nautiloid). B, Examples of load (kN) vs. displacement (mm) curves for each septal shape tested. Figure created in ggplot2 (Wickham 2016).

exponents) (Table 1). Therefore, our results do not support the hypothesis that increased septal complexity increased resistance to shell-crushing predators. When comparing peak loads sustained by different models, we observed that strength varied among models of both the same septal type (e.g., ceratitic) and different septal types (e.g., ceratitic vs. goniatitic) (Fig. 5A, Supplementary Fig. S3). While some models were consistently more resistant to crushing than others of the same septal type (e.g., *Diplomoceras* and *Schistoceras*), others were consistently less resistant (e.g., *Douvilleiceras*) than other models of the same septal type. This indicates that specific morphology had a greater influence on shell strength than the relative complexity of each septa when categorized by septal shape type. We

https://doi.org/10.1017/pab.2021.13 Published online by Cambridge University Press

TABLE 2. Dunn test significant pairwise comparisons ($p \leq 0.025$) of 3D-printed cephalopod models. Gray boxes show significant differences where the genus in the first row was stronger than the affiliated genus in the first column (e.g., *Diplomoceras* was significantly stronger than *Baculites*).

	Diplomoceras	*Baculites*	*Douvilleiceras*	*Otoceras*	*Pearylandites*	*Xenaspis*	*Schistoceras*	*Manticoceras*	*Diabloceras*	*Eifeloceras*	*Endoceras*	*Orthoceras*	Straight
Diplomoceras		0.0023	0		0.0142	0.0076	0.0002	0.0004	0.0005	0.0195		0.0173	0.0023
Baculites	0.0023			0.0124		0.0001	0			0.0178	0.0059	0.0005	0
Douvilleiceras	0		0.0124				0.0031						
Otoceras							0.0015						0.0142
Pearylandites	0.0142							0.0017	0.002				
Xenaspis		0.0076	0.0001					0	0	0.0021	0.0121		
Schistoceras		0.0002	0	0.0031	0.0015	0.0017	0					0.0044	0.0004
Manticoceras	0.0004					0.002	0					0.0053	0.0005
Diaboloceras	0.0005						0.0021						0.0195
Eifeloceras	0.0195		0.0178				0.0121						
Endoceras			0.0059										
Orthoceras		0.0173	0.0005					0.0044	0.0053				
Straight		0.0023	0		0.0142			0.0004	0.0005	0.0195			

obtained our results from models with standard laterally compressed cylindrical shell shapes. We note results might change significantly if future researchers model the same septa in coiled shells with differing degrees of whorl overlap that could buttress the shell against compressive forces (Hewitt and Westermann 1997). Our study stands as a basis for this future work.

Loading Curve Shapes.—The load-displacement curves were generally the same shape across different models. However, some models with ammonoid septal types (e.g., *Diplomoceras*, *Douvilleiceras*, *Diaboloceras*, and *Manticoceras*) exhibited small dips in load before peak load was reached, demonstrating precursor cracking in the model in the lead-up to failure (Fig. 5B–E). In contrast, nautiloid and straight septa models' loading curves were almost entirely monotonically increasing before peak load was reached. These observed cracks before complete failure in ammonoid septal shapes may demonstrate that the more complex shape of ammonoid septa could accommodate small cracks before shattering entirely, possibly creating more potential to escape a predator before the shell was completely compromised. Similar failure behaviors are observed in composite materials with many length scales, as having many length scales may change the mode of failure of the overall shape (Li et al. 2012). Additionally, the repetitious nature of fractal morphologies may allow for noncatastrophic failure to dissipate energy (Celli et al. 2003).

This study serves as a useful approximation for understanding the role of shape in isolation; however, the shell's microstructure, which we did not test here, undoubtedly also contributed to crack propagation. Previous authors have indicated that a predator would benefit more from attacking the body chamber of the shell (Klompmaker et al. 2009; Landman et al. 2012), where most of the soft tissue was located, rather than the phragmocone, where septa were located (although in some coiled taxa the body chamber wraps around much of the phragmocone). Predators likely would have preferentially attacked the body chamber of the shell if possible; however, it is also possible that large predators like marine reptiles would have encompassed the entirety of the shell in

https://doi.org/10.1017/pab.2021.13 Published online by Cambridge University Press

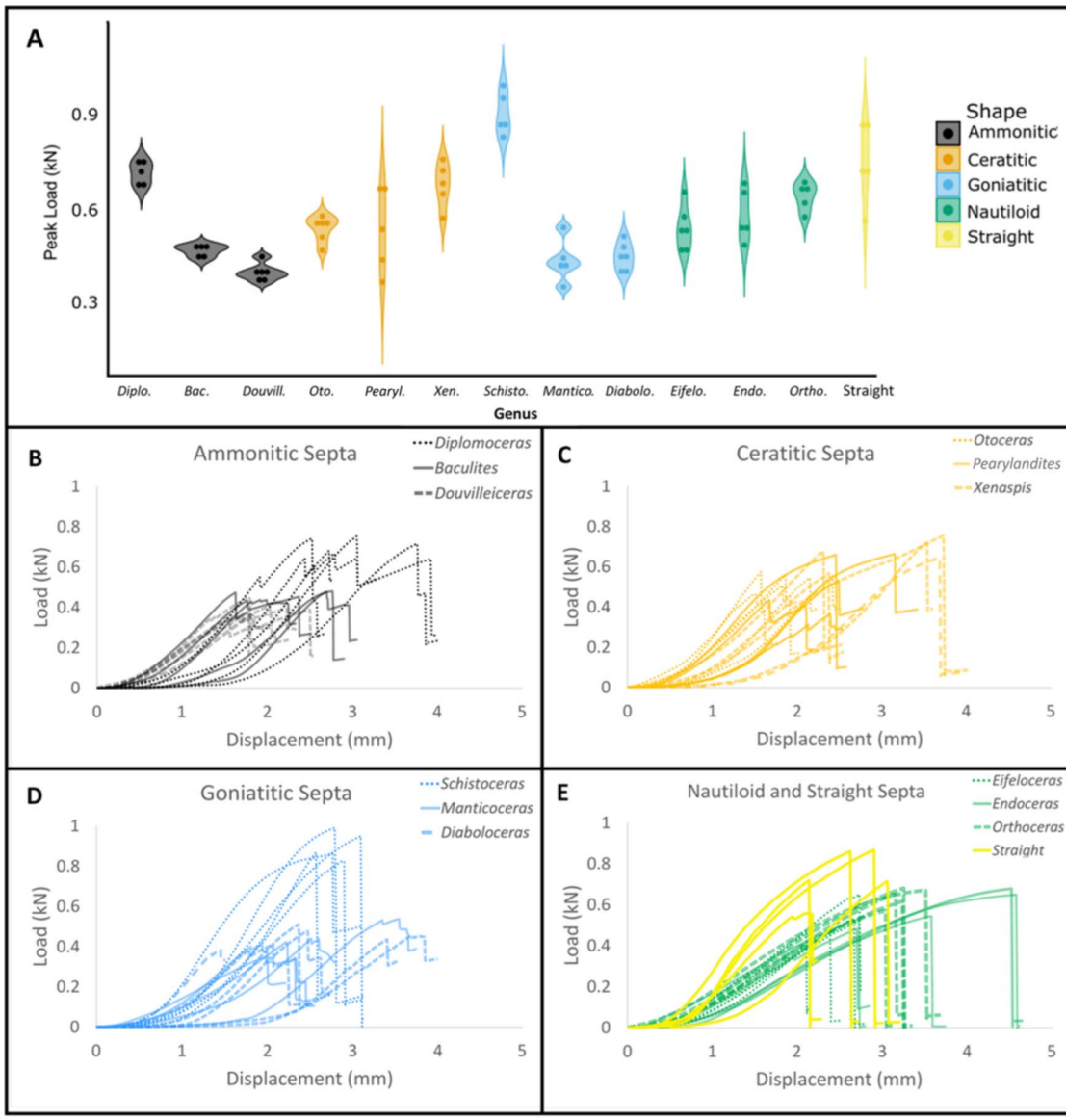


FIGURE 5. Peak loads of different septal morphologies. Peak loads sustained by models based on genera with different septal morphologies. A, Violin plot peak load (kN) sustained by models of different genera decreasing in septal complexity from left to right. Width of spindles indicated distribution of data points. Load (kN) versus displacement (mm) curves for B, ammonitic; C, ceratitic; D, goniatitic; E, nautiloid and straight septa. *Diplo.*, *Diplomoceras*; *Bac.*, *Baculites*; *Douvill.*, *Douvilleiceras*; *Oto.*, *Otoceras*; *Pearyl.*, *Pearylandites*; *Xen.*, *Xenaspis*; *Schisto.*, *Schistoceras*; *Mantico.*, *Manticoceras*; *Diabolo.*, *Diaboloceras*; *Eifelo.*, *Eifeloceras*; *Endo.*, *Endoceras*; *Ortho.*, *Orthoceras*.

their jaws without differentiating the location of the body chamber due to the difference between the size of the shell and their jaws. In instances such as these, the ability to dissipate energy by sustaining small cracks without completely shattering might give the ammonoid a better chance of escape. However, further testing would be required to analyze whether the fractal nature of ammonoid septa could have permitted small cracks before shattering or if even small cracks could have resulted in a fatal decrease in buoyancy.

Septal Morphology.—Throughout all tests, we observed cracks forming in septa before any

https://doi.org/10.1017/pab.2021.13 Published online by Cambridge University Press

cracking was seen in the outer shell (cylindrical tube). During experimental trials, we observed that cracks in ammonoid septa (ammonitic, ceratitic, and goniatitic) generally propagated from the lateral sides of the septum, where contact was made between the plate and the outer shell wall, toward the center of the septum before the center of the septum shattered (Fig 3A–I). By comparison, breaks in nautiloid walls occurred in many different locations, including the center of the septum, and there were many breaks toward the outer shell wall to the left or right of the septum center (Fig. 3J,K). In some cases, the septum shattered almost completely, very close to the outer wall. It is important to recall that to isolate the effects of septal shape, the siphuncle foramen location was kept the same in all models—toward the edge of the septum near the outer wall of the shell. This morphology is consistent with siphuncle foramen placement in ammonoids; however, in *Nautilus* shells, the siphuncle foramen is in the septal center. It is notable that nautiloids, the geologically older taxon, more commonly had this foramen placement, while ammonoids with complex septa appeared in the fossil record immediately with the siphuncle foramen located toward the outer wall of the shell (venter). As holes can behave as stress concentrators (Zirka et al. 2004), our results raise the possibility that the location of the siphuncle foramen in ammonoids may differ from that in nautiloids, because the center of the septum was the weakest part of the septum, although further testing is needed. Thus, locating a stress concentrator in an already weak portion of the shell may have been problematic. Moreover, the observation that fossil ammonoids show thickening of the center of the septum and thinning toward the outer walls is consistent with our findings that show that shattering frequently occurred in the center of a septum (Hewitt and Westermann 1997; Klug and Hoffmann 2015). Our models were generated using uniform thicknesses for extrusion to negate differences across taxa. Thickening of the center of the septum in life likely achieved reinforcement of this otherwise weak portion of the septum, as shell thickening increases shell strength (Lakowitz et al. 2008; Crofts and Summers 2014).

Limitations and Interpretation.—The fossilization process has rendered the functional morphology of ammonoid septa physically untestable without modeling and re-creation. While physical models are highly informative, condensing complex biological systems into testable units requires many constraints and assumptions. The results of the theoretical tests conducted for this study represent first-order approximations of natural systems. Here, we used brittle materials to approximate the failure of theoretical morphologies, rendered using computer-automated design programs. There was no whorl overlap considered in this model, because differing degrees of whorl overlap in different taxa would likely influence shell strength. Instead, we isolated septal shape without the complication of whorl overlap using a laterally compressed cylinder similar to an orthoconic shell (although without tapering). Designing the models in this way, we performed fundamental mechanical tests to understand complex natural morphologies. Therefore, the results of this experiment are to be interpreted as a theoretical test case to approximate the contribution of septal shape to shell strength when all other morphological characteristics are equal. We also maintained constant septal thickness to remove complicating variations between different taxa. These results serve as a stepping-stone for future experiments that may model more complex morphological variations, including whorl overlap, shell coiling, and changes in septal thickness.

While the resin we used does not possess the microstructure of real molluscan shells, which is known to mitigate crack propagation (Salinas and Kisailus 2013; Kulicki et al. 2015), the foremost breakage observed showed brittle behavior as expected in real shells. Moreover, the dominant direction of crack propagation was through 3D-printed layers, rather than along them, as seen in real shells. The appropriate behavior of the model materials allowed for relative comparisons to be made between shapes. The results of this study, and others using 3D-printed models (e.g., bivalves; Johnson 2020), are intended to demonstrate the relative strength imparted by different septal morphologies in otherwise identical shells;

https://doi.org/10.1017/pab.2021.13 Published online by Cambridge University Press

however, they are not intended to replicate the exact forces needed to break shells in life. Finally, this experiment also used flat plates to mimic flat crushing dentitions. Therefore, the results do not assess puncture or the interaction of multiple teeth applying point loads across the phragmocone. A quasistatic loading regime, without momentum, was used as a standardized mechanical test, which draws no conclusions about the ability of these models or complex septa to withstand impact. We highlight our assumptions and experimental limitations here, because these factors are especially important when designing models as a proxy to study the functional morphology of extinct organisms.

Conclusions

Paleontologists have long sought to understand what adaptive advantage might have driven increasing complexity in ammonoid septa. While past investigators have proposed many hypotheses to explain the functionality of these unique morphologies, these ideas have remained challenging to test, because there are no comparably complex modern shell morphologies. Here, we have developed an experiment using 3D printing to test the hypothesis that increasingly complex septa are more resistant to crushing predation. Using 3D-printed models, we were able to conduct destructive tests without damaging specimens or encountering the challenges of the fossilization process, which renders fossils untestable for various reasons (taphonomy, lithification, etc.). Our study represents the first physical test conducted to examine the strength of ammonoid septa in compression. We obtained three main findings through our selected samples: (1) Septal complexity does not correlate with overall strength measured by peak load in compression. Thus, this study does not support the hypothesis that predation drove the increased complexity of ammonoid septa when experimentally tested using flat crushing plates. (2) In some cases, we found preliminary evidence that ammonoid septal shapes (ammonitic, ceratitic, and goniatitic) may display small cracks before the shell's ultimate failure. This may indicate that these septa's fractal morphologies allow small cracks to dissipate energy before ultimate failure. If further testing shows that this is a repeated occurrence, the self-similarity of more complex septa may permit more ductile behavior in compression by sustaining small breaks before catastrophic failure. (3) The location of crack propagation and ultimate breakage in ammonoid septa (repeatably in the center of a septum) and nautiloid septa (more variable, some centered, some toward the outer edge of the shell) raises an interesting evolutionary proposition for the placement of the siphuncle foramen in these taxa. Because holes can act as stress concentrators, this suggests that the center of a septum may have been a detrimental placement for a siphuncle foramen in an ammonoid should it be compressed—concentrating stress at the weak center of a septum. Thus, the mechanics of shell compression may have had a selective influence on the placement of this morphology in ammonoids. The experimental observation of relatively weak septal centers also gives a mechanical understanding of the variation in septal thickness in ammonoid fossils. The center of the septum is thicker than the outer edges, likely reinforcing a weak area. Our results indicate that shell-crushing predation was unlikely to have driven the evolution of increasingly complex septa. However, these findings raise the question of whether septal thickness and the placement of the siphuncle foramen were likely constrained for biomechanical reasons. Much work remains to understand how these unique shapes imparted shell strength and what additional factors may have driven their increasing complexity (buoyancy, liquid transport, etc.). This study demonstrates the usefulness of empirical testing enabled by rapidly developing technology, which will surely create exciting and novel opportunities to increase our understanding of the evolution of form and function in many taxa.

Acknowledgments

We thank P. Dodson, D. Jerolmack, and H. Pfefferkorn for helpful comments and discussions. We also thank D. Vann and S. Szewczyk for assistance with lab equipment. This research

https://doi.org/10.1017/pab.2021.13 Published online by Cambridge University Press

was in part supported by funding through the National Science Foundation Graduate Research Fellowship Program (DGE-1845298). Additionally, internal funding was provided by the Greg and Susan J. Walker Foundation and the Summer Research Stipend in Paleontology (Department of Earth and Environmental Science at the University of Pennsylvania). Delaware Valley Paleontological Society also supported this project through the Paul Bond Scholarship fund. The authors declare no competing interests.

Data Availability Statement

Data available from the Dryad Digital Repository: https://doi.org/10.5061/dryad.pvmcvdnk6.

Supplementary Figure S1. Materials test of rigid resin.

Supplementary Figure S2. Generalized depiction of the box method of fractal analysis modified from Peterman and Barton (2019).

Supplementary Figure S3. Septal shape and shell strength with genera grouped by shape.

Literature Cited

Arkell, W. J., W. J. Furnish, B. Kummel, A. K. Miller, R. C. Moore, O. H. Schindewolf, and C. W. Wright. 1957. Mollusca 4, Cephalopoda, Ammonoidea. Part L of R. C. Moore, ed. Treatise on invertebrate paleontology. Geological Society of America, New York, and University of Kansas, Lawrence.

Blender Online Community. 2020. Blender 2.76—a 3D modelling and rendering package. Stichting Blender Foundation, Amsterdam. http://www.blender.org.

Boyajian, G., and T. Lutz. 1992. Evolution of biological complexity and its relation to taxonomic longevity in the Ammonoidea. Geology 20:983–986.

Buckland, W. 1836. Geology and mineralogy considered with reference to natural theology. Treatise VI. The Bridgewater treatise on the power, wisdom, and goodness of God as manifested in the Creation. W. Pickering, London.

Celli, A., A. Tucci, L. Esposito, and C. Palmonari. 2003. Fractal analysis of cracks in alumina–zirconia composites. Journal of the European Ceramic Society 23:469–479.

Checa, A. G., J. H. E. Cartwright, I. Sanchez-Almazo, J. P. Andrade, and F. Ruiz-Raya. 2015. The cuttlefish *Sepia officinalis* (Sepiidae, Cephalopoda) constructs cuttlebone from a liquid-crystal precursor. Scientific Reports 5:1513.

Crofts, S. B., and A. P. Summers. 2014. How to best smash a snail: the effect of tooth shape on crushing load. Journal of the Royal Society Interface 11:20131053.

Daniel, T. L., B. S. Helmuth, W. B. Saunders, and P. D. Ward. 1997. Septal complexity in ammonoid cephalopods increased mechanical risk and limited depth. Paleobiology 23:470–481.

Ebel, K. 1992. Mode of life and soft body shape of heteromorph ammonites. Lethaia 25:179–193.

Hassan, M. A., G. E. Westermann, R. A. Hewitt, and M. A. Dokainish. 2002. Finite-element analysis of simulated ammonoid septa (extinct Cephalopoda): septal and sutural complexities do not reduce strength. Paleobiology 28:113–126.

Hewitt, R. A., and G. E. G. Westermann. 1997. Mechanical significance of ammonoid septa with complex sutures. Lethaia 30:205–212.

Johnson, E. 2021. Breaking down shell strength: inferences from experimental compression and future directions enabled by 3D printing. Biological Reviews. doi: 10.1111/brv.12692.

Johnson, E., and A. Carter. 2019. Defossilization: a review of 3D printing in experimental paleontology. Frontiers in Ecology and Evolution 7:430.

Johnson, E. H. 2020. Experimental tests of bivalve shell shape reveal potential tradeoffs between mechanical and behavioral defenses. Scientific Reports 10:1–12.

Jones, D. L. 1963. Upper Cretaceous (Campanian and Maastrichtian) ammonites from southern Alaska. U.S. Geological Survey Professional Paper 432:1–53.

Kauffman, E. G., and R. V. Kesling. 1960. An Upper Cretaceous ammonite bitten by a mosasaur. Contributions from the Museum of Paleontology, University of Michigan 15:193–248.

Kerr, J. P., and P. H. Kelley. 2015. Assessing the influence of escalation during the Mesozoic Marine Revolution: shell breakage and adaptation against enemies in Mesozoic ammonites. Palaeogeography, Palaeoclimatology, Palaeoecology 440:632–646.

Keupp, H. 2012. Atlas zur paläopathologie der cephalopoden. Fachrichtung Paläontologie, Institut für Geologische Wissenschaften, Freie Universität Berlin.

Klompmaker, A. A., N. A. Waljaard, and R. H. Fraaije. 2009. Ventral bite marks in Mesozoic ammonoids. Palaeogeography, Palaeoclimatology, Palaeoecology 280:245–257.

Klug, C., and R. Hoffmann. 2015. Ammonoid septa and sutures. Pp. 45–90 *in* C. Klug, D. Korn, K. De Baets, I. Kruta, and R. H. Mapes, eds. Ammonoid paleobiology: from anatomy to ecology. Springer, Dordrecht, Netherlands.

Klug, C., E. Meyer, U. Richter, and D. Korn. 2008. Soft-tissue imprints in fossil and Recent cephalopod septa and septum formation. Lethaia 41:477–492.

Kolmann, M. A., S. B. Crofts, M. N. Dean, A. P. Summers, and N. R. Lovejoy. 2015. Morphology does not predict performance: jaw curvature and prey crushing in durophagous stingrays. Journal of Experimental Biology 218:3941–3949.

Kulicki, C., and H. Mutvei. 1988. Functional interpretation of ammonoid septa. Pp. 713–718 *in* J. Wiedmann and J. Killmann, eds. Cephalopods—present and past. Schweizerbart'sche Verlagsbuchhandlung, Stuttgart, Germany.

Kulicki, C., K. Tanabe, N. H. Landman, and A. Kaim. 2015. Ammonoid shell microstructure. Pp. 321–357 *in* C. Klug, D. Korn, K. De Baets, I. Kruta, and R. H. Mapes, eds. Ammonoid paleobiology: from anatomy to ecology. Springer, Dordrecht, Netherlands.

Lakowitz, T., C. Brönmark, and P. E. R. Nyström. 2008. Tuning in to multiple predators: conflicting demands for shell morphology in a freshwater snail. Freshwater Biology 53:2184–2191.

Landman, N. H., W. A. Cobban, and N. L. Larson. 2012. Mode of life and habitat of scaphitid ammonites. Geobios 45:87–98.

Landman, N. H., S. Goolaerts, J. W. Jagt, E. A. Jagt-Yazykova, M. Machalski, and M. M. Yacobucci. 2014. Ammonite extinction and nautilid survival at the end of the Cretaceous. Geology 42:707–710.

Landman, N. H., S. Goolaerts, J. W. Jagt, E. A. Jagt-Yazykova, and M. Machalski. 2015. Ammonites on the brink of extinction: diversity, abundance, and ecology of the Order Ammonoidea at the Cretaceous/Paleogene (K/Pg) boundary. Pp. 497–553 *in* C. Klug, D. Korn, K. De Baets, I. Kruta, and R. H. Mapes, eds. Ammonoid paleobiology: from macroevolution to paleogeography. Springer, Dordrecht, Netherlands.

https://doi.org/10.1017/pab.2021.13 Published online by Cambridge University Press

Lemanis, R. 2020. The ammonite septum is not an adaptation to deep water: re-evaluating a centuries-old idea. Proceedings of the Royal Society of London B 287:20201919.

Lemanis, R., and I. Zlotnikov. 2018. Finite element analysis as a method to study molluscan shell mechanics. Advanced Engineering Materials 20:1700939.

Lemanis, R., D. Korn, S. Zachow, E. Rybacki, and R. Hoffmann. 2016a. The evolution and development of cephalopod chambers and their shape. PLoS ONE 11:e0151404.

Lemanis, R., S. Zachow, and R. Hoffmann. 2016b. Comparative cephalopod shell strength and the role of septum morphology on stress distribution. PeerJ 4:e2434.

Lewy, Z. 2003. Reply to Checa and to Hewitt and Westermann. Journal of Paleontology 77:796–798.

Li, Y., C. Ortiz, and M. C. Boyce. 2012. Bioinspired, mechanical, deterministic fractal model for hierarchical suture joints. Physical Review E 85:031901.

Mapes, R. H., and D. T. Chaffin. 2003. Predation on cephalopods. Pp. 177–213 *in* P. Kelley, M. Kowalewski, H. Michal, and A. Thor, eds. Predator–prey interactions in the fossil record. Springer, Boston.

Mutvei, H. 1967. On the microscopic shell structure in some Jurassic ammonoids. Neues Jahrbuch für Geologie und Paläontologie–Abhandlungen 129:157–166.

Newell, N. D. 1949. Phyletic size increase, an important trend illustrated by fossil invertebrates. Evolution 3:103–124.

Peterman, D. J., and C. C. Barton. 2019. Power scaling of ammonitic suture patterns from Cretaceous Ancyloceratina: constraints on septal/sutural complexity. Lethaia 52:77–90.

Peterman, D. J., C. N. Ciampaglio, R. C. Shell, and M. M. Yacobucci. 2019. Mode of life and hydrostatic stability of orthoconic ectocochleate cephalopods: hydrodynamic analyses of restoring moments from 3D printed, neutrally buoyant models. Acta Palaeontologica Polonica 64:441–460.

Pia, J. 1923. Über die ethologische Bedeutung einiger Hauptzüge in der Stammesgeschichte der Cephalopoden. Annalen des Naturhistorischen Museums in Wien, 50–73.

R Core Team. 2020. R: a language and environment for statistical computing. R Foundation for Statistical Computing, Vienna, Austria. https://www.r-project.org.

Richter, A. E. 2009. Ammoniten-Gehäuse mit Bissspuren. Berliner Paläobiologische Abhandlungen 10:297–305.

Romer, A. S. 1966. Vertebrate paleontology. University of Chicago Press, Chicago.

Salinas, C., and D. Kisailus. 2013. Fracture mitigation strategies in gastropod shells. JOM 65:473–480.

Saunders, W. B. 1995. The ammonoid suture problem: relationships between shell and septum thickness and suture complexity in Paleozoic ammonoids. Paleobiology 21:343–355.

Schulp, A. S. 2005. Feeding the mechanical mosasaur: what did *Carinodens* eat? Netherlands Journal of Geosciences 84:345–357.

Stein, R. A., C. G. Goodman, and E. A. Marschall. 1984. Using time and energetic measures of cost in estimating prey value for fish predators. Ecology 65:702–715.

Tajika, A., A. Nützel, and C. Klug. 2018. The old and the new plankton: ecological replacement of associations of mollusc plankton and giant filter feeders after the Cretaceous? PeerJ 6:e4219.

Tajika, A., N. H. Landman, R. Hoffmann, R. Lemanis, N. Morimoto, C. Ifrim, and C. Klug. 2020. Chamber volume development, metabolic rates, and selective extinction in cephalopods. Scientific Reports 10:2950.

Takeda, Y., K. Tanabe, T. Sasaki, and N. H. Landman. 2016. Durophagous predation on scaphitid ammonoids in the Late Cretaceous Western Interior Seaway of North America. Lethaia 49:28–42.

Teichert, C. 1967. Major features of cephalopod evolution. Pp. 162–210 *in* C. Teichert and E. L. Yochelson, eds. Essays in paleontology and stratigraphy: R. C. Moore commemorative volume. University of Kansas Press, Lawrence.

Teichert, C., R. C. Moore, and D. E. Nodine Zeller. 1964. Rhyncholites. Pp. K467–K484 *in* Cephaloda Nautiloidea. Part K of R. C. Moore, ed., Treatise on invertebrate paleontology. Geological Society of America, New York, and University of Kansas Press, Lawrence.

Tintori, A. 1998. Fish biodiversity in the marine Norian (Late Triassic) of northern Italy: the first Neopterygian radiation. Italian Journal of Zoology 65:193–198.

Vermeij, G. J. 1977. The Mesozoic marine revolution: evidence from snails, predators and grazers. Paleobiology 3:245–258.

von Huene, F. R. 1956. Paläontologie und Phylogenie der niederen Tetrapoden. Guastav Fischer, Jena, Germany, 716.

Vullo, R. 2011. Direct evidence of hybodont shark predation on Late Jurassic ammonites. Naturwissenschaften 98:545–549.

Wickham, H. 2016. ggplot2: elegant graphics for data analysis. Springer-Verlag New York.

Wright, C. W. 1996. Mollusca 4, Cretaceous Ammonoidea. Part L (revised) of R. L. Kaesler, ed. Treatise on invertebrate paleontology, vol. 4. Geological Society of America, Boulder, Colo. and University of Kansas, Lawrence.

Zirka, A. I., M. P. Malezhik, and I. S. Chernyshenko. 2004. Stress concentration in an orthotropic plate with a circular hole under dynamic loading. International Applied Mechanics 40:226–230.

https://doi.org/10.1017/pab.2021.13 Published online by Cambridge University Press